Electric fields at solid-liquid interfaces: Insights from molecular dynamics simulation

Julia A. Nauman,[1] Dylan Suvlu,[1] and Adam P. Willard[1] [1]Department of Chemistry, Massachusetts Institute of Technology, Cambridge, Massachusetts, USA, 02139; email:awillard@mit.edu

In this manuscript, we explore the electrostatic environment of the interface between a solid and a dilute electrolyte solution, with an emphasis on the electric field profiles that these systems produce. We review the theoretical formalism that connects electrostatic potential profiles, electric field profiles, and charge density fields. This formalism has served as the basis for our understanding of interfacial electric fields and their influences on microscopic chemical and physical processes. Comparing various traditional models of interfacial electrostatics to the results of molecular dynamics (MD) simulation yields mutually inconsistent descriptions of the interfacial electric field profile. We present MD simulation results demonstrating that the average electric field profiles experienced by particles at the interface differ from the properties of traditional models and from the fields derived from the mean charge density of atomistic simulations. Furthermore, these experienced electric field profiles are species-dependent. Based on these results, we assert that a single unifying electrostatic potential profile - the gradient of which defines a single unifying electric field profile - cannot correctly predict the electrostatic forces that act on species at the interface.

CONTENTS

I. INTRODUCTION

Solid-liquid interfaces provide a catalytic environment for many important chemical and physical processes. The catalytic potency of these environments stems largely from their tendency to produce strong, persistent electric fields.[1–3] These fields push and pull on ions, electrons, protons, and molecules to help them find transition states and overcome activation barriers. Over a century of scientific effort has been aimed at understanding the properties of these fields, how they can be controlled, and how they can be leveraged to enable advances in the chemical sciences.[1–12] However, despite this effort, surprisingly little is known about the structure of the electric field profiles at these interfaces.

Here, we consider the equilibrium properties of the electric field profile at the interface between a solid surface and a dilute electrolyte solution (e.g., ionic concentration of $\sim 10^0 - 10^{-2}$ M). Due to the physical consequences of ionic screening, these fields are only appreciable within a narrow region of space extending less than 1nm into the liquid.[4,13,14] This molecular scale region is extremely difficult to isolate via experiment, which is why our current physical understanding lags significantly behind that for bulk systems. Electrochemical measurements report accurately on the electrostatic potential differences on either side of a solid-liquid interface,[15,16] Interfacial electric field profiles are then derived from theoretical models that prescribe the shape of the electrostatic potential profile that spanning the interface, as illustrated in Fig. 1.

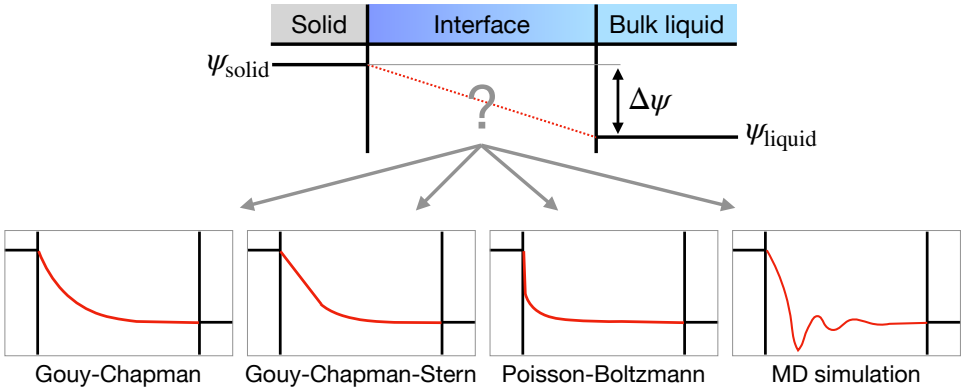

FIG. 1. Electrochemical measurements report on the potential difference, $\Delta\Psi$, across a solid-liquid interface. Theoretical models are required to describe the shape of the interfacial potential profile (red lines). The electric field profile is then given by the negative gradient of the electrostatic potential. Different models thus predict different interfacial electric field profiles.

In the absence of reliable experimental probes, our best current tool for validating these theoretical models is molecular dynamics (MD) simulation. In this manuscript, we highlight the ability of MD simulation to provide molecular-scale insight into the properties of interfacial electric field profiles. We also show how MD simulation can be utilized to test the reliability of standard theoretical models. To accomplish this, rather than excerpting from an array of different simulation studies in the literature, we present previously unpublished results from an unremarkable yet illustrative model system. This model is similar to those appearing throughout the literature.[17–19] By utilizing this model we hope to provide generalizable physical insight while maintaining consistency and clarity across the various sections.

The manuscript is organized as follows. First, in the following section, we review the formalism connecting charge density profiles, electrostatic potentials, and electric fields. Then, in Sec. III we provide a brief review of the experimental, theoretical, and computational studies that have led to our current understanding of the interfacial electrostatic environment. In Sec. IV we present the details of the simulation model. We use this model to explore the properties of the interfacial potential, presented in Sec. V, and interfacial electric fields, presented in Sec. VI. Finally, in Sec. VII, we conclude and comment briefly on the scientific outlook of this field.

II. THE FOUNDATIONAL RELATIONSHIP BETWEEN POTENTIALS, ELECTRIC FIELDS, AND CHARGE DENSITY PROFILES

The interfacial electric field profile is typically defined as the negative gradient of a spatially varying electrostatic potential landscape. In solution-phase systems, this seemingly straightforward relationship can lead to confusion because there are multiple related yet non-equivalent ways that the electrostatic potential can be defined. Although these different definitions are thermodynamically consistent, they predict very different interfacial field profiles. These profiles are consequential because they motivate our molecular-level understanding of interfacial chemical processes.

Varying definitions of the electrostatic potential arise due to differences in the assumed role of solvent in interfacial electrostatics (*e.g.*, implicit or explicit), or in whether the potential is meant to act on a hypothetical charged species introduced to the system or on an

existing species within the system. In this section, we present three common definitions of the electrostatic potential that highlight these differences. In doing so, we will establish a notation that will allow these different potentials to be easily distinguished, compared, and contrasted.

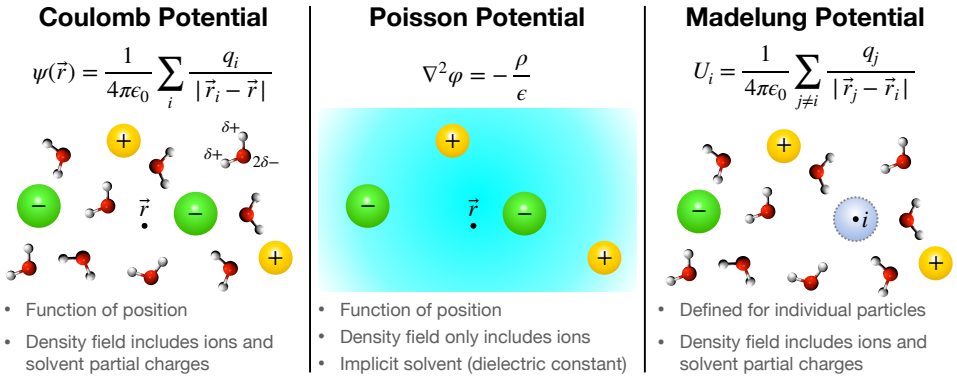

FIG. 2. Schematic representation of Coulomb, Poisson, and Madelung potentials, as formulated in this manuscript.

A. The Coulomb Potential, ψ

Coulomb's law establishes a general definition of the electrostatic potential, ψ. Specifically, the Coulomb potential at position $\vec{r}$ due to a point charge q_i at position $\vec{r}_i$ is given by, $\psi(\vec{r}) \propto q_i/|\vec{r} - \vec{r}_i|$, where the constant of proportionality is $(4\pi\epsilon_0)^{-1}$ and ϵ_0 is the vacuum permittivity. Contributions to this potential are additive, and thus in a field of multiple point charges, the Coulomb potential is a sum of single point-charge contributions,

$$\psi(\vec{r}) = \frac{1}{4\pi\epsilon_0}\sum_i \frac{q_i}{|\vec{r} - \vec{r}_i|}. \tag{1}$$

Alternately, this potential can be expressed as an integral over a continuous charge density field, $\rho(\vec{r})$, as,

$$\psi(\vec{r}) = \frac{1}{4\pi\epsilon_0}\int d\vec{r}' \frac{\rho(\vec{r}')}{|\vec{r} - \vec{r}'|}, \tag{2}$$

where $\rho(\vec{r})$ is the net charge density at position $\vec{r}$. To relate Eqs. 1 and 2 we recognize that for a point charge system, $\rho(\vec{r}) = \sum_i q_i \delta(\vec{r}_i - \vec{r})$, where $\delta(x)$ is the Dirac delta function.

The Coulomb potential quantifies electrostatic contributions to a system's potential energy. More specifically, the electrostatic potential energy of a point charge systems is,

$$E_{\text{Coul}} = \frac{1}{4\pi\epsilon_0} \sum_{i<j} \frac{q_i q_j}{|\vec{r}_i - \vec{r}_j|}, \tag{3}$$

where the summation is taken over all unique pairs of particles, and thus the potential energy change to create a charge of magnitude q at position $\vec{r}$ is given by,

$$\Delta E_{\text{Coul}} = q\psi(\vec{r}). \tag{4}$$

A general definition of the electric field, $\vec{E}(\vec{r})$, follows from this relationship. Specifically, the force experienced by a charge q at position $\vec{r}$ is,

$$\vec{F}_q(\vec{r}) \equiv q\vec{E}(\vec{r}) = -q\nabla\psi(\vec{r}). \tag{5}$$

In other words, the electric field at any given position is given by the negative local gradient of the electrostatic potential landscape.

B. The Poisson Potential, φ

The Coulomb potential dictates a differential relationship between the electrostatic potential and charge density field, ρ. This relationship is formalized by the Poisson equation,

$$\nabla^2\varphi = -\frac{\rho}{\epsilon}, \tag{6}$$

where we have taken φ to denote the *Poisson potential* and ϵ is the dielectric constant of the medium in units of the vacuum permittivity (ϵ_0). Notably, if ρ is taken to be the explicit charge density field (as in Eq. 2), and $\epsilon = 1$, then φ and ψ are formally identical. More commonly, however, φ is formulated in terms of an implicit or reduced charge density field, describing only contributions from ionic species (omitting neutral solvent molecules), and ϵ is set to the dielectric constant of the solution. In this case, φ represents an effective electrostatic potential for the ionic species in solution and is thus not generally equivalent to ψ.

For the purpose of this review, we will reserve the notation φ for cases where solvent's partial charge distribution is omitted from $\rho(\vec{r})$ and captured instead in terms of ϵ (*i.e.*, a

dielectric continuum), and ψ to indicate the case where $\epsilon = 1$ and the solvent partial charges contribute directly to $\rho(\vec{r})$.

Although Eq. 6 applies to systems of arbitrary dimensionality, for interfacial systems the potential is typically resolved along a particular axis, *e.g.*, the axis extending perpendicular to the plane of a solid-liquid interface. In this case, the Poisson equation is given by,

$$\frac{d^2\varphi(z)}{dz^2} = -\frac{\rho(z)}{\epsilon}, \tag{7}$$

where z denotes the axis of interest, $\rho(z)$ is the projection of the three-dimensional charge density field along this axis, and $\varphi(z)$ is the one-dimensional Poisson potential profile.

If $\rho(z)$ represents the mean charge density profile, then $q\varphi(z)$ is the mean potential energy associated with creating a fictive charge, q, at position z. As such, the gradient in φ can be interpreted as the mean electric field acting on such a fictive charge. Herein, we will denote this electric field as E_φ, *e.g.*,

$$E_\varphi(z) = -\frac{d\varphi(z)}{dz}. \tag{8}$$

This quantity provides a physically intuitive description of the effective Coulombic driving forces that are present in a system. However, these forces do not necessarily represent the mean forces actually experienced by a given charged species in the system. This is because φ and its gradients are native to the influence of a species on its local environment. For example, the local environment of an ion is enriched in counter charge and in addition can include a strongly bound and highly polarized solvation shell. The influences of these molecular effects are integrated out of the mean charge density profile and thus may not be apparent in $\varphi(z)$ or its gradients.

C. The Madelung potential, U_i

The Madelung potential quantifies the potential experienced by a specific particle within the system. Specifically, the Madelung potential for particle i in a system of point charges is given by,

$$U_i = \frac{1}{4\pi\epsilon_0} \sum_{j \neq i} \frac{q_j}{|\vec{r}_i - \vec{r}_j|}, \tag{9}$$

where the summation is carried out over all other particles within the system, q_j is the charge on particle j. Unlike the Poisson and Coulomb potentials, the Madelung potential accounts for the influence of a species on its local electrostatic environment.

The full Coulomb energy of a system can be expressed in terms of Madelung potentials as,

$$E_{\text{Coul}} = \frac{1}{2}\sum_i q_i U_i. \tag{10}$$

This equation can be used to derive a relationship between the Madelung potential and the local electric field. The Coulomb force on particle i is defined as $\vec{F}_i = -dE_{\text{Coul}}/d\vec{r}_i$, which leads to the expression,

$$\vec{F}_i = -q_i\left(\frac{dU_i}{d\vec{r}_i}\right), \tag{11}$$

where q_i is the charge on particle i. Comparing this expression to Eq. 5 leads to,

$$\vec{E}_i = -\left(\frac{dU_i}{d\vec{r}_i}\right). \tag{12}$$

This relationship serves to motivate an interpretation of U_i as the local (in both space and time) electrostatic potential acting on a given particle i.

D. Thermal fluctuations of the Madelung potential and its associated electric fields

The Madelung potential, as defined in Eq. 9, is a function of the nuclear configuration of the system. Therefore, thermal motions of particles in the system will lead to fluctuations in U_i. At equilibrium, these fluctuations can be quantified in terms of a probability distribution function, $P(U_\alpha)$, where α is the species type for particle i. The width of $P(U_\alpha)$ can be specified by the variance, $\sigma_\alpha^2 = \langle(\delta U_i)^2\rangle$, where $\delta U_i = (U_i - \langle U_\alpha\rangle)$. For simulation studies, this quantity can be evaluated by studying the statistics of U_i for an ensemble of particles of type α sampled from equilibrium simulations. These fluctuations drive charge thermalization and are directly related to the solvent reorganization energy of Marcus theory.[20,21]

The long-range nature of Coulomb interactions presents a challenge when studying the fluctuations of U_i. Specifically, due to the r^{-1} scaling, U_i for individual configurations does not converge over a finite length scale. While the strength of contributions to U_i decreases as r^{-1}, the volume element (and thus the number of contributing species) associated with a given distance increases as r^2. The consequences of this scaling competition can be appreciated by considering a radially-resolved formulation of the Madelung potential for a

spherically symmetric particle,

$$U_i = \frac{1}{\epsilon_0}\int_0^\infty drrQ(r) \equiv \int_0^\infty dr\tilde{u}_i(r), \tag{13}$$

where $Q(r)$ denotes the total net charge at a distance r from particle i. In essence, the quantity, $\tilde{u}_i(r)$ quantifies the contribution to U_i originating from particles at a specific distance r from particle i.

The failure of U_i to converge in real space can be demonstrated with a lattice model of an uncorrelated Gaussian density field. Specifically, consider the Madelung potential, U_0, of a central site within a three-dimensional cubic lattice. Each lattice site is assigned a random charge q_i drawn from a Gaussian distribution, $P(q_i) \propto \exp(-q_i^2)$. The value of $\tilde{u}_0(r)$ for several random charge configurations is plotted in Fig. 3A. As this model illustrates, $\tilde{u}_0(r)$ contributes random noise with constant amplitude at all radial distances. Thus, the value of U_i for a given charge configuration is determined primarily by long-ranged uncorrelated noise, and not (as one might incorrectly intuit) the fluctuations of the local electrostatic environment. Therefore, Madelung potential quantities such as $P(U_\alpha)$ and $\langle(\delta U_\alpha)^2\rangle$ are not reliable reporters of the local electrostatic environment. Notably, $\langle U_i\rangle$ reports on the structure of the local electrostatic environment because the uncorrelated random noise at long range averages to zero.

In contrast, the electric field decays more rapidly with distance (as r^{-2}) and therefore converges over finite length scales. This can be quantified in terms of the radial-resolved components of the Madelung electric field vector $\vec{E}_i = \int dr\vec{\varepsilon}_i(r)$, where,

$$\vec{\varepsilon}_i(r) = -\frac{d}{d\vec{r}_i}\left(\frac{1}{4\pi\epsilon_0}\sum_{j\neq i}\frac{q_j}{|\vec{r}_i - \vec{r}_j|}\delta(r - r_{ij})\right) = -d\tilde{u}_i(r)/d\vec{r}_i. \tag{14}$$

Figure 3B contains a plot of $\tilde{E}_i(r) = |\vec{\varepsilon}_i(r)|$ for the same Gaussian field model, demonstrating convergence over finite distance. In other words, the properties of $\vec{E}_i$ are primarily determined by the local environment, even for individual configurations. Thus the statistics of the Madelung electric field are useful in reporting on the properties of the local electrostatic environment.

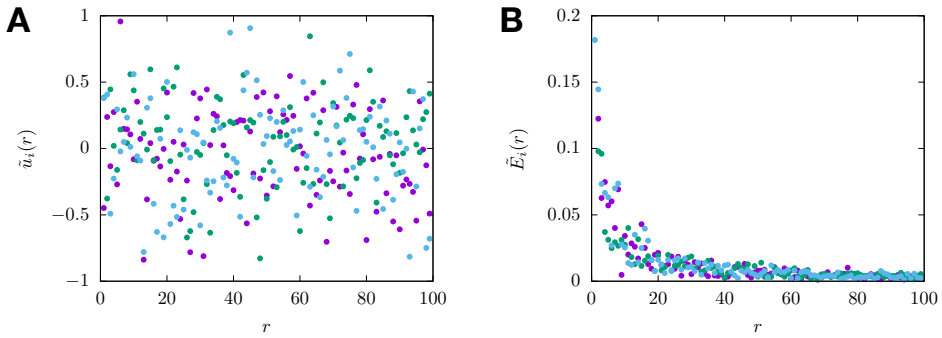

FIG. 3. A lattice model of a random Gaussian charge density field. Radial contributions to the (A) Madelung potential and (B) electric field vector, as defined in Eqs. 13 and 14, respectively. Different point colors correspond to different random configurations of the charge density field. Results are presented in arbitrary units.

III. THE BASIS OF OUR UNDERSTANDING OF INTERFACIAL ELECTROSTATIC PROPERTIES

Due to the importance of solid-liquid interfaces in the chemical sciences, they have been the target of a broad range of scientific studies for more than a century.[4,22,23] Despite all of this attention, much still remains to be uncovered about the electrostatic properties of solid-liquid interfaces at the molecular scale. In this section, we review the essential experimental, theoretical, and computational techniques that have been utilized to study these systems and highlight the physical insight they have provided.

A. Insight from experiment

Electrochemical and spectroscopic techniques are capable of probing various aspects of solid-liquid interfaces but provide limited insight into the molecular scale characteristics of interfacial electric fields. Typical electrochemical techniques infer interfacial properties based primarily on current-voltage relationships.[24,25] The benefit of electrochemical techniques is that they are capable of directly isolating the interface; however, the measurements average over macroscopic surfaces and thus lack molecular detail. Molecular scale interfacial properties (e.g., electric field profiles) must be inferred using theoretical models which often include unverified assumptions.[4,26] Furthermore, the interpretation of electrochemical

measurement tends to assume a homogeneous interfacial structure, yet it has often been speculated that surface imperfections can play an outsized role in interfacial chemistry and thus in facilitating the flow of current.[27]

On the other hand; modern spectroscopic techniques are capable of reporting on molecular details, however, isolating the comparatively tiny interfacial signal from that of the bulk is a general challenge affecting the spectroscopic community.[28–32] In addition, spectroscopists must account for the sometimes significant interactions of pump and probe pulses with the solid.[33] In some cases, these interactions can be harnessed to amplify interfacial signal.[30,34] Despite these challenges, our ability to measure the molecular properties of solid-liquid interfaces continues to improve.[30,35,36]

Some of the first insight into interfacial electrostatics were derived from measurements of interfacial differential capacitance, quantifying the change in solid surface charge with applied voltage, and electrocapillarity, measuring the surface tension of electrode-electrolyte solution interfaces.[22,37,38] These measurements led to the development of the concept of an electric double-layer (EDL),[23,39] which persists today as a cornerstone of our microscopic understanding of solid-liquid interfaces.

Another class of electrochemical measurement is derived from the transport properties of the solution at the solid-liquid interface, such as flow electrification[40,41] and pressure-wave propagation.[42,43] Insights gained from these techniques are based on the concept that the motion or flow of an electrolyte solution at a solid surface depends on the space charge characteristics of the liquid-solid interface. Interfacial electrostatic profiles can be derived from these experiments, but the shape of the profiles cannot be determined directly by the experiment but must be assumed in modeling efforts.

Spectroscopic techniques such as Raman and IR vibrational spectroscopy can be applied to monitor molecular species within the liquid interface or bound directly to the solid surface. Spectral signatures that depend on the external electric field can be monitored and analyzed to infer the electric field properties of the interface.[44–47] X-ray-based techniques, such as X-ray photoelectron spectroscopy can be applied similarly to study the interfacial electrochemical environment.[48–53] In this case, insight derives from the fact that the electronic energies are sensitive to the value of their local atomic environment or electrostatic potential. These techniques provide specific information about adsorption sites and adsorbate order, adsorbate configurational geometry, and surface band structures.[54,55] Sum frequency

and second-harmonic generation spectroscopy are capable of isolating interfacial signal and have been used to identify changes in spectral properties of interfacial molecules.[56–58]

Devices utilizing a surface force apparatus can be used to provide information about molecular interfacial structure.[59,60] This type of experiment have provided clear evidence of molecular layering at interfaces, for example as manifest in long-range charge oscillations emerging from solid ionic-liquid interfaces.[61,62] Simiarly, atomic force microscopy can be used to report on the electrostatic profiles at pristine solid-liquid interfaces.[63] This class of techniques provides concrete evidence of the manifestation of molecular excluded volume effects at interfaces, which are neglected in most standard theories of interfacial electrostatic profiles.

B. Insight from theory

Much of our physical understanding of the electrostatic properties of solid-liquid interfaces derives from the pioneering developments of Gouy, Chapman, Stern, and Grahame, over 100 years ago.[23,39] These pioneers popularized the concept of the electric double-layer (EDL), which describes the microscopic structure of the space-charge region, *i.e.*, $\rho(z)$, that spontaneously forms at the liquid interface. This concept and the models that describe the EDL have been essential in our ongoing efforts to interpret a wide array of electrochemical measurements and in generating predictions for how chemical processes can be controlled through changes in applied potential or electrolyte composition.[4,5,14]

The EDL structure prescribes the spatial variations in the interfacial charge density and thus determines the shape of the interfacial potential profile and its associated electric fields. EDL models predict experimentally measurable properties, such as the interfacial differential capacitance,[64–66] and thus can be validated or parameterized through experimental feedback.[65] However, many of the specific details about EDL structure cannot yet be uniquely determined.[25] Accordingly, uncertainty remains about which EDL model is "correct" or appropriate for interpreting a given experiment.

The foundational assumption for traditional EDL models is that the solution is well described as a rapidly relaxing continuum with a well-defined dielectric constant, to represent the screening properties of the neutral solvent molecules, and ionic strength to represent the concentration of solvated ionic species. In standard Gouy-Chapman theory, the potential

profile is determined by solving the Poisson-Boltzmann (PB) Equation,

$$\frac{d\varphi(z)}{dz^2} = -\frac{1}{\epsilon}\sum_{\alpha} q_\alpha n_0^{(\alpha)} e^{-\beta q_\alpha \varphi(z)}, \tag{15}$$

where the summation is taken over all unique types of species, q_α is the charge on species type α, and $n_0^{(\alpha)}$ is the bulk number density of species α. The exponential term asserts that the position-dependent concentration of species α is Boltzmann distributed according to the charge-potential interaction. For dilute solutions, and systems with V_0 lower than about 0.5mV, the exponent in Eq. 15 can be expanded to first order in φ to yield an interfacial potential profile that decays approximately exponentially with a specific form,[67]

$$\varphi(z) \approx V_0 e^{-(z-z_0)/\lambda_{\mathrm{D}}}, \tag{16}$$

where V_0 is the potential at the liquid boundary, z_0 indicates the position of the electrode surface, and λ_{D} is the familiar Debye screening length.

Stern hypothesized the presence of a solvent (or ionic) monolayer separating the solid surface from the electrolyte solution, *i.e.*, the Stern layer.[68] Within this layer of molecular width, the potential drops linearly before reverting to the exponential form of Eq. 15. However, PB theory is only valid for dilute solutions. It is missing the short range correlations due to steric interactions as well as long range electrostatic correlations. These shortcomings in PB theory are the motivation behind subsequent development in more advanced approaches including statistical field theory,[69–73] classical density functional theory (cDFT),[74,75] integral equations,[76] and Landau-Ginzburg type functionals.[77–80] Validation of these theories by comparison to experiment or molecular simulation continues to provide insight into the nature of the EDL.

C. Insight from simulation

Over the last 20 years, largely due to the increase in availability and power of scientific computing platforms, simulation studies have been increasingly important in guiding our understanding of solid-liquid interfacial systems.[6,14,17,81–87] Despite this, challenges still remain due to the multi-scale nature of these systems. Systems on the order of 1-10nm are required to represent the bulk and to account for heterogeneity (*e.g.*, in surface structure). At the same time, high physical resolution is required to describe molecular and atomic

polarization, and chemical reactivity. And yet changes in molecular electronic structure and reactivity are too expensive to describe more than a handful of individual molecules or surface atoms. Classcial MD simulations can be extended to represent bulk systems, but they rely on force fields that are parameterized for the bulk and thus may fail to accurately represent the molecular structure of the interface.

The gap between first-principles and classical simulation is slowly closing due to the development of hybrid approaches, such as QM/MM,[86,88,89] and generalized Langevin equation approaches.[90] In addition, machine learning interatomic potentials (MLIPs) are improving the accuracy and efficiency of molecular simulations.[91–95] However, MLIPs for interfacial systems are still in development and traditional ab initio and classical force field simulations remain a valuable tool in investigating the EDL.

Some of the first ab initio simulations of the metal/water interface were conducted over 20 years ago.[96,97] Increases in computational power have expanded the time and length scales available to these simulation techniques but they remain computationally expensive.[85,86,98] Consequently, the solvent is often treated implicitly with a polarizable continuum model,[99,100] or explicitly but at a coarser resolution in QM/MM models[86,88,89,101]. Additional developments relate to how the interface is electrified, either with half-cell models such as grand canonical DFT[102–104], or full-cell models like in finite field MD[105]. Despite the continued improvements in methodology the computational cost of these techniques prohibit the accessible time scales and sampling of relevant electrolyte configurations. As a result, classical force field simulations have emerged as a powerful compromise between atomistic detail and computational cost.

Siepmann and Sprik developed a force field model that allows metal atom charges to fluctuate at every time step maintaining electrode equipotential.[106] This method was subsequently utilized to simulate electrochemical cells[17,107–109] and has since been integrated into software packages such as MetalWalls,[110] and LAMMPS.[18] The technique was recently used to calculate the capacitance[111,112], and water structure and reorientation dynamics[113,114] at electrified graphene interfaces. It also has been extended with the Thomas-Fermi model to tune the metallicity of electrode atoms[115]. The method has demonstrated utility as a compromise between atomistic detail and computational expense[17].

IV. AN ILLUSTRATIVE AND HIGHLY TUNABLE MODEL SYSTEM

The physical picture that we present below is derived from a model system of an aqueous electrolyte solution confined between two parallel constant potential electrodes, as illustrated in Fig. 4. This system is not cutting edge in terms of accuracy or scale, yet it is sufficient to converge the statistics of interfacial electrostatic properties and efficient enough to explore systematic variations in parameters such as applied potential, temperature, and electrolyte composition (such parameters are easily manipulated in experimental studies). In this section, we describe this model system.

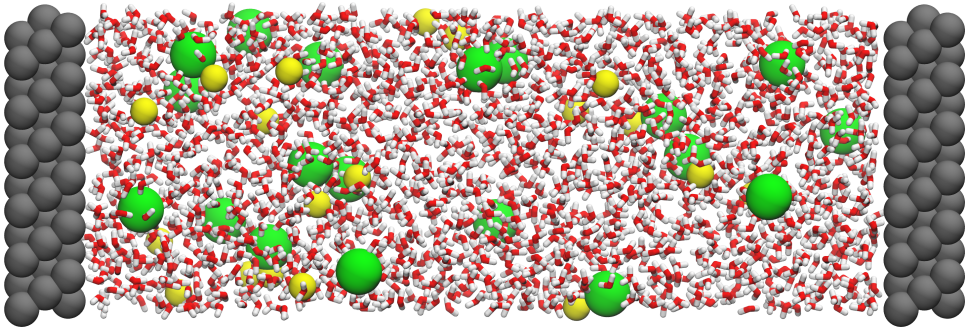

FIG. 4. Simulation snapshot of the aqueous electrolyte-electrode system utilized in this manuscript. The grey particles represent electrode atoms, the left-hand and right-hand electrodes are held at constant potentials of $-V_{\text{ext}}$ and $+V_{\text{ext}}$, respectively. Water molecules, depicted in red and white, solute Na^+ and Cl^- ions, depicted as yellow and green spheres, respectively, at a concentration of approximately 0.5M.

The model system depicted in Fig. 4 has dimensions 27.72 Å × 28.81 Å × 90.52 Å. The x- and y-dimensions of the system are periodically replicated, while the aperiodic z-dimension of the system runs perpendicular to the planar electrode surfaces. The positions of the electrode atoms remain fixed in an FCC lattice throughout the simulation, and the charges of the electrode atoms are assigned using a fluctuating charge constant potential method,[106,107,116] which maintains the atoms in the left electrode at a constant potential of V_{ext} and the atoms in the right electrode at a constant potential of $-V_{\text{ext}}$. By construction, the reference potential for the electrodes, $V_{\text{ext}} = 0$, corresponds to the potential of zero charge (PZC). The constant potential method is implemented using the ELECTRODE package[18] in LAMMPS.[117] Water molecules are represented using the SPC/E water model,[118] and Na^+

and Cl^- ions are also modeled with a classical force field.[119] The system was evolved in the canonical ensemble at a temperature of 298 K for 15 ns, and the last 10 ns of the 15 ns trajectory was used for the data analysis presented in this manuscript.

V. ELECTROSTATIC POTENTIALS AT THE AQUEOUS LIQUID-SOLID INTERFACE

In this section, we demonstrate the ability of classical MD simulation to resolve the properties of the electrostatic potential at an aqueous electrolyte-electrode interface at scales that cannot be probed experimentally. Simulation allows us to evaluate the assumptions that underlie traditional theoretical models and to identify the physical consequences when those assumptions break down. Such insight can improve our ability to analyze experimental results and enrich our interpretation of data.

In the subsection below, we compare the potential profiles predicted by Gouy-Chapman theory to those calculated from simulation data. We find little consistency. We highlight in particular the non-triviality of representing water's interfacial dielectric response and comment on the manifestation of this response in the Madelung potential profiles. Then, in the subsequent subsection, we present the statistics of the Madelung potential fluctuations, highlighting their species- and position-dependence, as well as their finite-size effects.

A. The average interfacial potential profile

We begin by considering a 0.5M aqueous solution of NaCl confined between opposing electrodes held at constant potential with $V_{\text{ext}} = 0.5\text{V}$, as described in Sec. IV.

Figure 5 contains a plot of a variety of interfacial potential profiles at the positive electrode interface. This includes the prediction of Poisson-Boltzmann theory (Eq. 15), Gouy-Chapman theory (Eq. 16), $\Psi_{\text{GC}}(z)$, as well as the average Coulomb ($\psi(z)$), Poisson ($\varphi(z)$), and Madelung ($U_\alpha(z)$) potentials calculated from equilibrium simulation data. As a reminder, for these results, $\psi(z)$ was calculated by solving Eq. 7 when $\rho(z)$ is the full charge density and $\epsilon = 1$, and $\varphi(z)$ was calculated by solving Eq. 7 when $\rho(z)$ is the ionic charge density and $\epsilon = \epsilon_{\text{int}} > 1$.

At the $V_{\text{ext}} = 0.5\text{V}$ electrode, the familiar Gouy-Chapman potential profile decays expo-

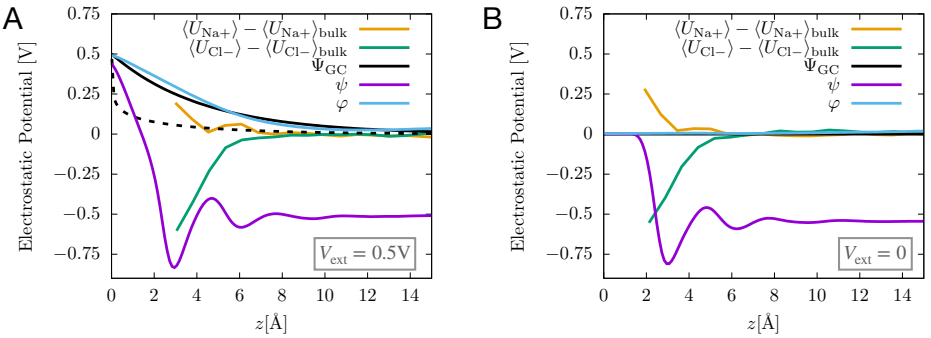

FIG. 5. Mean electrostatic potential profiles predicted from theory and simulation for interfacial systems with electrode potentials of (A) $V_{\mathrm{ext}} = 0.5V$ and (B) $V_{\mathrm{ext}} = 0$. The Madelung potential profiles $\langle U_\alpha \rangle$ are shifted for clarity by their average values in the bulk, $\langle U_{\mathrm{Cl-}} \rangle_{\mathrm{bulk}} = 7.8V$ and $\langle U_{\mathrm{Na+}} \rangle_{\mathrm{bulk}} = -8.8V$.

nentially over a length of about 1 nm to a bulk value of $\Psi_{\mathrm{GC}} = 0$. We observe that this smooth decay is roughly captured by the Poisson potential φ, for which water is modeled as a dielectric continuum. Therefore, the spatial distribution of counter-ionic charge in the vicinity of the interface conforms to the physical picture implied by Gouy-Chapman theory. That is, the z-dependent chemical potential for dilute ions is determined by the energetics of the charge interacting with the screened electrode. Note that the difference between Poisson-Boltzmann and Gouy-Chapman theory (dashed and solid black lines in Fig. 5) reveal that the linear approximation utilized to get from Eq. 15 to Eq. 16 is not valid for the parameters of this system (e.g., applied potential and electrolyte concentration). The agreement between Ψ_{GC} and φ thus reveals that the effective strength of ion-potential interactions are small compared to $k_{\mathrm{B}}T$. Apparently, the polarization of interfacial water molecules, and their excluded volume, lead to a much lower effective potential for the electrolyte species. It is also worth mentioning that in order to generate this Poisson potential profile it is necessary to input a value of $\epsilon_{\mathrm{int}} \approx 5$. We comment further on the subtleties of capturing water's dielectric properties later in this subsection.

The Coulomb potential, ψ, in which water's partial charges are accounted for explicitly in the mean charge density field differs qualitatively from the predictions of Gouy-Chapman theory. These differences arise due to the molecular nature of water and therefore signal a breakdown in the dielectric continuum assumption.[120] The primary differences are pronounced oscillations, due to molecular layering at the solid surface, and an overall interfacial

potential drop $\Delta V \neq V_{\text{ext}}$, due to water's preference to orient with its hydrogens pointing toward the electrode under unbiased conditions.[121] The qualitative details of this potential profile depend on the characteristics of the force field. However, a significant difference from Gouy-Chapman theory is very likely a general characteristic of all-atom systems.

The differences between ψ and φ are especially apparent when $V_{\text{ext}} = 0$. In that case, Ψ_{GC} predicts a featureless profile, which is similarly captured by φ. However, even under unbiased conditions, ψ predicts a non-trivial interfacial potential profile. This unbiased profile highlights the degree to which water's molecular nature can affect the interfacial electrostatic environment.

Figure 5 also includes plots of the Madelung potential, $U_\alpha(z)$, for $\alpha = \text{Cl}^-$ and $\alpha = \text{Na}^+$. These profiles (shifted vertically for clarity) exhibit values that are large in magnitude $\sim 7 - 9\text{V}$ due to the fact that the local solvation environment of an ion is enriched in counter charge (a la Debye-Huckel theory). These profiles vary at the interface, indicating the electrostatic potential profile experienced by these ions as they approach the electrode surface. Remarkably, these Madelung potential profiles differ from each other, indicating that either ion experiences the electrostatic environment in its own way, and both differ from φ and ψ, indicating that neither the Poisson nor the Coulomb potential profiles accurately represent effective potential experienced by these species. This mutually inconsistent set of potential profiles lead to ambiguity in predicting the mean interfacial electric fields. We will attempt to resolve this ambiguity in Sec. VI.

It is interesting to consider what role, if any, the solvent dielectric plays in determining the shape of the interfacial potential profile and its associated electric fields. From the comparison between ψ and φ we can conclude that several significant features are lost in going from an atomistic description of the solvent to a dielectric continuum approximation. Whether these features are relevant to the microscopic chemical and physical processes that occur at the interface is not obvious and indeed not evident when further examining the profiles $U_\alpha(z)$. For instance, $U_{\text{Na+}}(z)$ exhibits some evidence of interfacial oscillations, albeit with reduced amplitude relative to ψ. In contrast, the potential $U_{\text{Cl}-}(z)$ appears to exhibit no interfacial oscillations.

A surprising aspect of water's interfacial dielectric response is the necessity to assign a value of $\epsilon_{\text{int}} = 5$. This value is significantly lower than the bulk value, $\epsilon_{\text{water}} \approx 78$, indicating that water's screening response is significantly reduced at the solid-liquid interface.

This observation is not without precedent - multiple studies using different techniques have identified similarly low values of ϵ_{int} for water.[122,123]

B. Thermal fluctuations in the Madelung potential

To gain a deeper understanding of the microscopic electrostatic properties of aqueous solutions, we study the fluctuations in the Madelung potential. We quantify these fluctuations in terms of probability distribution functions, $P(U_\alpha)$. The equilibrium probability distribution functions, $P(U_\alpha)_{\text{bulk}}$, for $\alpha =$Na$^+$ and Cl$^-$ for a periodically replicated bulk system with the same force field and electrolyte concentration are plotted in Fig. 6A. These distributions indicate that fluctuations in U_i are roughly Gaussian with means of $\langle U_{\text{Na+}} \rangle \approx -8.5V$ and $\langle U_{\text{Cl}-} \rangle \approx 8.5V$ and variances of $\langle (\delta U_i)^2 \rangle_{\text{Na+}} \approx 0.22$ and $\langle (\delta U_i)^2 \rangle_{\text{Cl}-} \approx 0.19$. The differences in these means and variances arise due to differences in the solvation structure of the two different ionic species. The values of $\langle U_\alpha \rangle$ differ from those presented in Fig. 7, because the long range nature of Coulomb interaction causes these values to depend on the details of the simulation cell (periodic versus interfacial).

The quantitative features of these distributions are highly system dependent. Most notably, the variance of the distributions are system-size dependent. Figure 6 contains a plot of the variance of $P(U_\alpha)$ calculated in periodically replicated bulk systems of different sizes. We observe that the variance increases systematically with system size, indicating that the long-range nature of the Coulomb interactions (highlighted in Sec. II D) also affects the equilibrium statistics of U_α.

In systems with constant potential boundaries (such as the electrodes we employ), the variance in $P(U_\alpha)$ exhibits a pronounced position dependence. Specifically, it has been noted multiple times in the literature that electrostatic potential fluctuations systematically narrow for species approaching the surface of a constant potential surface (such as the electrodes we employ in our simulations).[21,124] This narrowing is illustrated in Fig. 6C, which shows the variance of $P(U_\alpha)$ for several species in solution as a function of their position between the two constant potential electrodes. At all positions in the nanoscale system, even well beyond the Debye screening length, the fluctuations in U_α increase away from the electrodes. This is, yet again, a manifestation of the long-range nature of Coulomb interactions that can complicate the physical interpretation of these microscopic statistical properties.

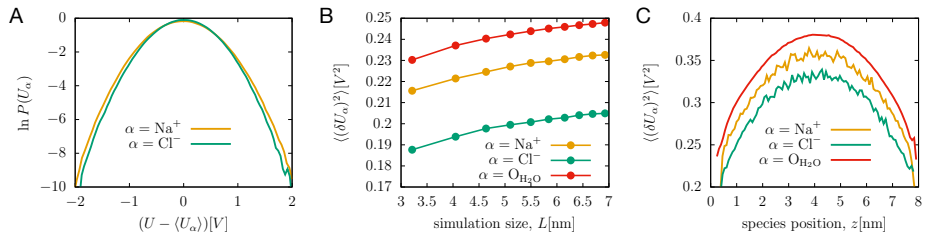

FIG. 6. The statistics of Madelung potential fluctuations in aqueous electrolyte solutions. (A) The probability distribution, $P(U_\alpha)$, for Na^+ and Cl^- in a periodically replicated bulk aqueous solution. (B) Variance of $P(U_\alpha)$ for species in a periodically replicated bulk system with simulation cell side length L. (C) Variance of $P(U_\alpha)$ for members of a species α located at position z in an aqueous electrolyte solution confined between constant potential electrodes. The positive and negative electrode positions are located at $z = 0$ and $z = 8.15$nm, respectively.

VI. ELECTRIC FIELDS AT THE AQUEOUS LIQUID-SOLID INTERFACE

The previous section presents several variants of the electrostatic potential profile at the interface between an electrode and a dilute aqueous electrolyte solution. In principle, the interfacial electric field is given by the negative gradient of the electrostatic potential. However, as we demonstrated, these various potential profiles differ qualitatively. In this section, we utilize the same simulation data to calculate the electric fields experienced by species in solution both in the bulk and at the electrode interface. By analyzing these calculations we can identify which potential profile, if any, is most consistent with the electric fields that act on electrolyte species.

This section is organized similarly to the previous section. First, we analyze the average Madelung electric field profiles and compare them to the predictions of theory and simulation. Then, in the following subsection, we consider the electric field fluctuations and how they are affected by the presence of an interface.

A. The average interfacial electric field profile

Figure 7 contains a plot of the average profiles for the z-component of the electric field vector, E_z, for the various potential definitions. For the Gouy-Chapman (Ψ_{GC}), Coulomb (ψ), and Poisson (φ) potentials, we define the electric field as the negative gradient of

the potential in the z-direction. As with the potential profiles, these electric field profiles differ significantly from each other. When $V_{\text{ext}} = 0.5\text{V}$, the Poisson and Gouy-Chapman fields are roughly similar, predicting mean interfacial fields with magnitudes $|E_z|$ less than about 0.1V/Å. In contrast, the field derived from the Coulomb potential predicts alternating positive and negative fields with much larger magnitudes of $|E_z|$ less than about 0.5V/Å. When $V_{\text{ext}} = 0\text{V}$, both Gouy-Chapman and the Poisson fields are predicted to be negligible, while the Coulomb field profile continue to exhibit high amplitude oscillations, similar to those for the case with $V_{\text{ext}} = 0.5\text{V}$.

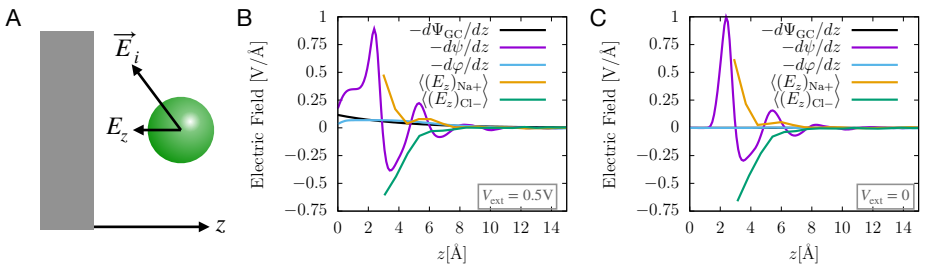

FIG. 7. (A) The quantity E_z is the z-component of the Madelung electric field vector, $\vec{E}_i$. Mean electric field profiles predicted from theory and simulation for interfacial systems with electrode potentials of (B) $V_{\text{ext}} = 0.5V$ and (C) $V_{\text{ext}} = 0$.

The green and yellow lines in Fig. 7 represent the average z-component of the electric field acting on Na^+ and Cl^- as calculated directly from MD simulation data. The physical implications of these plots are that a cation species experiences increasingly positive fields and a negative species experiences increasingly negative fields as it approaches the interface from the bulk. These fields are large in magnitude relative to those predicted by Gouy-Chapman theory. Surprisingly, they are both repulsive, implying that the electrostatic environment of the electrode interface has the net effect of repelling both the anionic and cationic species. The negative electrode is similarly repulsive to both species. The repulsion manifests despite the presence of image charge interactions, which are attractive and fully captured by our model. Clearly, the operational electrostatic forces at the interface are species-specific. This phenomenology can not be represented by a single universal interfacial electric field (or potential) profile.

The Madelung electric fields report direction on the electrostatic forces that atoms and molecules experience in solution and at the interface. For this reason, the Madelung electric

field is most relevant to our understanding of molecular and chemical dynamics at the molecular scale. It follows that the electrostatic potential derived from a single average net charge density field, including Gouy-Chapman and related theories, provides an incomplete and potentially erroneous depiction of the fields that act on species at the interface. This is not to say that this class of theories are not useful. Indeed, Poisson and Gouy-Chapman profiles provide a wealth of physical intuition into the thermodynamic consequences of Coulombic interactions. Nonetheless, the act of conditioning the electrostatic calculation on the presence of a species has a significant qualitative impact on the apparent properties of the potential and electric field profiles.

B. Thermal fluctuations in the Madelung electric field

In this subsection, we analyze the fluctuations in the Madelung electric fields for both Na^+ and Cl^- species in the bulk and at the solid-liquid interface. We highlight two main points. First, the electric field experienced by species in solution exhibits broad fluctuations about the mean. Second, unlike the fluctuations in the U_α, the width of electric field fluctuations exhibits no significant dependence on system size or system position. These points support the use of Madelung electric fields as a robust and transferable probe of the local electrostatic environment.

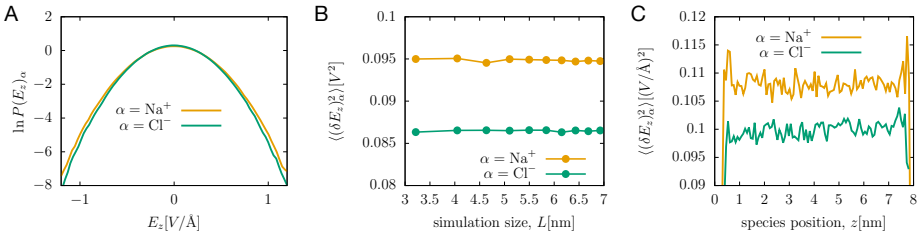

FIG. 8. The statistics of Madelung electric field fluctuations in aqueous electrolyte solutions. (A) The probability distribution, $P(E_z)$, for Na^+ and Cl^- in a periodically replicated bulk aqueous solution. (B) Variance of $P(E_z)$ for species in a periodically replicated bulk system with simulation cell side length L. (C) Variance of $P(E_z)$ for members of a species α located at position z in an aqueous electrolyte solution confined between constant potential electrodes. The positive and negative electrode positions are located at $z = 0$ and $z = 8.15$nm, respectively.

Figure 8A presents a plot of $P(E_z)$ for Na^+ and Cl^- species in a bulk periodic replicated

simulation of a 0.5M aqueous electrolyte solution. In the bulk, the average field is zero, and so the average of any component of the electric field vector is also zero. We observe that the statistics of field fluctuations for Na^+ and Cl^- are similar but not identical. These subtle differences are due to differences in the solvation structure of these two different species. The notable observation from this calculation is that the widths of these distributions indicate a standard deviation of about 0.3V/Å. Evidently, at least in this model of an aqueous electrolyte solution, the strength of fluctuating fields experienced by species in solution can be quite large at any given instance, yet these strong fields persist only fleetingly.

Figures 8B and C contain plots analogous to the panels in Fig. 6. We observe that due to the local nature of electric fields, the statistics of their fluctuations do not include the artifacts associated with changes in system size or species position relative to the electrode. Oxygen atoms exhibit an analogous trend, but have a significantly larger variance due to the dipolar nature of the water molecule, so we omit that data here.

VII. SYNOPSIS AND OUTLOOK

Solid-liquid interfaces produce strong electric fields that serve to facilitate a broad array of important chemical and physical processes. Our molecular-level understanding of these processes, and how they are affected by the interface, depends on the spatial distribution of these interfacial electric fields. These electric field profiles are typically derived from theoretical models or simulation studies of the mean charge density field. The field profiles predicted by this general approach do not represent the electric field profiles experienced by species in the system and therefore should not be applied to develop physical insight into interfacial chemical reaction rates or mechanisms.

Classical MD simulation is an excellent tool for refining our general physical understanding of interfacial electrostatic properties. In particular, simulations enable direct evaluation of the assumptions that underlie standard theoretical models. The ubiquitous assumption that solvent is a simple dielectric continuum is not generally applicable at interfaces. At the interface, solvent dielectric is both anisotropic (different in parallel and perpendicular directions) and spatially varying. Alternately, the solvent dielectric response can be represented as an explicit finite width contribution to the charge density field, resulting in significant deviations from Gouy-Chapman-like theories.

MD simulations reveal that the interfacial electric field profiles that are experienced by particles at the solid-liquid interface are species-dependent. These species-dependent electric field profiles are consistent with the gradients of the species-dependent Madelung potential profiles. Therefore, resolving Madelung potential profiles (and their associated electric fields) is important for understanding the effects of the interfacial electrostatic environment on chemical processes at the molecular scale.

The species-dependent nature of interfacial electric fields has some important and largely unexplored implications. If different species are subject to different average electric field profiles, then the influence of electrostatic forces on processes that involve the simultaneous motion of multiple particles can be complicated and difficult to intuit. Basing one's intuition on the characteristics of a single potential profile may lead to erroneous predictions. Despite these challenges, this complexity has an up-side. A species-dependent electric field landscape admits a large design space for manipulating interfacial chemistry.

At the time and length scales that characterize individual chemical reactions (the *molecular scale*), the electrostatic potential landscape is rugged and ever-fluctuating due to the thermal motion of charged species both near and far. These fluctuations are essential for enabling rare events involving charge dynamics. Due to the long-range nature of Coulomb interactions, which lead to pronounced finite-size effects, these electrostatic fluctuations are best quantified in terms of Madelung electric fields.

Many developments are needed to improve our understanding of interfacial electric fields and their influence on chemical processes. Due to the physical importance of the Madelung potential and its associated fields, experimental techniques capable of probing species-dependent Madelung potentials are needed. Such experiments would provide a much needed source of feedback for validating and improving simulation methods and force fields. The exceedingly broad potential and electric field fluctuations observed in classical simulation may reflect a limitation in the use of non-polarizable point-charge force fields. Extended simulations with more accurate molecular charges would be valuable in contextualizing the results of classical MD simulations. Finally, theoretical studies exploring the consequences of species-specific electric fields on interfacial chemical dynamics could motivate further experimental and simulation studies.

DISCLOSURE STATEMENT

The authors are not aware of any affiliations, memberships, funding, or financial holdings that might be perceived as affecting the objectivity of this review.

ACKNOWLEDGMENTS

This work was supported by U.S. Department of Energy through Grant No. DE-SC0018094.

REFERENCES

[1]S. Shaik, D. Danovich, J. Joy, Z. Wang, and T. Stuyver, "Electric-Field Mediated Chemistry: Uncovering and Exploiting the Potential of (Oriented) Electric Fields to Exert Chemical Catalysis and Reaction Control," Journal of the American Chemical Society **142**, 12551–12562 (2020).

[2]S. Ciampi, N. Darwish, H. M. Aitken, I. Díez-Pérez, and M. L. Coote, "Harnessing electrostatic catalysis in single molecule, electrochemical and chemical systems: A rapidly growing experimental tool box," Chemical Society Reviews **47**, 5146–5164 (2018).

[3]F. Che, J. T. Gray, S. Ha, N. Kruse, S. L. Scott, and J.-S. McEwen, "Elucidating the Roles of Electric Fields in Catalysis: A Perspective," ACS Catalysis **8**, 5153–5174 (2018).

[4]G. Gonella, E. H. G. Backus, Y. Nagata, D. J. Bonthuis, P. Loche, A. Schlaich, R. R. Netz, A. Kühnle, I. T. McCrum, M. T. M. Koper, M. Wolf, B. Winter, G. Meijer, R. K. Campen, and M. Bonn, "Water at charged interfaces," Nature Reviews Chemistry **5**, 466–485 (2021).

[5]P. Li, Y. Jiao, J. Huang, and S. Chen, "Electric Double Layer Effects in Electrocatalysis: Insights from Ab Initio Simulation and Hierarchical Continuum Modeling," JACS Au (2023), 10.1021/jacsau.3c00410.

[6]R. E. Warburton, A. V. Soudackov, and S. Hammes-Schiffer, "Theoretical Modeling of Electrochemical Proton-Coupled Electron Transfer," Chemical Reviews **122**, 10599–10650 (2022).

[7]V. V. Welborn, L. Ruiz Pestana, and T. Head-Gordon, "Computational optimization of electric fields for better catalysis design," Nature Catalysis **1**, 649–655 (2018).

[8]I. Ledezma-Yanez, W. D. Z. Wallace, P. Sebastián-Pascual, V. Climent, J. M. Feliu, and M. T. M. Koper, "Interfacial water reorganization as a pH-dependent descriptor of the hydrogen evolution rate on platinum electrodes," Nature Energy **2**, 1–7 (2017).

[9]V. R. Stamenkovic, D. Strmcnik, P. P. Lopes, and N. M. Markovic, "Energy and fuels from electrochemical interfaces," Nature Materials **16**, 57–69 (2017).

[10]Y. Y. Birdja, E. Pérez-Gallent, M. C. Figueiredo, A. J. Göttle, F. Calle-Vallejo, and M. T. M. Koper, "Advances and challenges in understanding the electrocatalytic conversion of carbon dioxide to fuels," Nature Energy **4**, 732–745 (2019).

[11]A. S. Bandarenka and M. T. M. Koper, "Structural and electronic effects in heterogeneous electrocatalysis: Toward a rational design of electrocatalysts," Journal of Catalysis 50th Anniversary Special Issue, **308**, 11–24 (2013).

[12]P. Sebastián-Pascual, Y. Shao-Horn, and M. Escudero-Escribano, "Toward understanding the role of the electric double layer structure and electrolyte effects on well-defined interfaces for electrocatalysis," Current Opinion in Electrochemistry **32**, 100918 (2022).

[13]J. O. Bockris and A. K. Reddy, *Modern electrochemistry 2B: electrodics in chemistry, engineering, biology and environmental science* (Springer Science & Business Media, 1998).

[14]M. Becker, P. Loche, M. Rezaei, A. Wolde-Kidan, Y. Uematsu, R. R. Netz, and D. J. Bonthuis, "Multiscale Modeling of Aqueous Electric Double Layers," Chemical Reviews **124**, 1–26 (2024).

[15]S. W. Boettcher, S. Z. Oener, M. C. Lonergan, Y. Surendranath, S. Ardo, C. Brozek, and P. A. Kempler, "Potentially Confusing: Potentials in Electrochemistry," ACS Energy Letters **6**, 261–266 (2021).

[16]J. Lyklema, "Interfacial Potentials: Measuring the Immeasurable?" Substantia , Vol 1 No 2 (2017) (2017).

[17]L. Scalfi, M. Salanne, and B. Rotenberg, "Molecular simulation of electrode-solution interfaces," Annual Review of Physical Chemistry **72**, 189–212 (2021).

[18]L. J. Ahrens-Iwers, M. Janssen, S. R. Tee, and R. H. Meißner, "Electrode: An electrochemistry package for atomistic simulations," The journal of chemical physics **157** (2022).

[19]G. Pireddu, C. J. Fairchild, S. P. Niblett, S. J. Cox, and B. Rotenberg, "Impedance of nanocapacitors from molecular simulations to understand the dynamics of confined electrolytes," Proceedings of the National Academy of Sciences **121**, e2318157121 (2024).

[20]J. Blumberger and M. Sprik, "Redox Free Energies from Vertical Energy Gaps: Ab Initio Molecular Dynamics Implementation," in *Computer Simulations in Condensed Matter Systems: From Materials to Chemical Biology Volume 2*, Vol. 704, edited by M. Ferrario, G. Ciccotti, and K. Binder (Springer Berlin Heidelberg, Berlin, Heidelberg, 2006) pp. 481–506.

[21]A. M. Limaye, W. Ding, and A. P. Willard, "Understanding attenuated solvent reorganization energies near electrode interfaces," The Journal of Chemical Physics **152** (2020).

[22]H. v. Helmholtz, "Studien über electrische grenzschichten," Annalen der Physik **243**, 337–382 (1879).

[23]D. L. Chapman, "Li. a contribution to the theory of electrocapillarity," The London, Edinburgh, and Dublin philosophical magazine and journal of science **25**, 475–481 (1913).

[24]A. M. Limaye, J. S. Zeng, A. P. Willard, and K. Manthiram, "Bayesian data analysis reveals no preference for cardinal Tafel slopes in CO2 reduction electrocatalysis," Nature Communications **12**, 703 (2021).

[25]K. Doblhoff-Dier and M. T. M. Koper, "Electric double layer of Pt(111): Known unknowns and unknown knowns," Current Opinion in Electrochemistry **39**, 101258 (2023).

[26]J. Wu, "Understanding the Electric Double-Layer Structure, Capacitance, and Charging Dynamics," Chemical Reviews **122**, 10821–10859 (2022).

[27]R. Majee, S. Parvin, Q. Arif Islam, A. Kumar, B. Debnath, S. Mondal, S. Bhattacharjee, S. Das, A. Kumar, and S. Bhattacharyya, "The Perfect Imperfections in Electrocatalysts," The Chemical Record **22**, e202200070 (2022).

[28]F. Vidal and A. Tadjeddine, "Sum-frequency generation spectroscopy of interfaces," Reports on Progress in Physics **68**, 1095 (2005).

[29]H.-F. Wang, L. Velarde, W. Gan, and L. Fu, "Quantitative Sum-Frequency Generation Vibrational Spectroscopy of Molecular Surfaces and Interfaces: Lineshape, Polarization, and Orientation," Annual Review of Physical Chemistry **66**, 189–216 (2015).

[30]C. L. Brosseau, A. Colina, J. V. Perales-Rondon, A. J. Wilson, P. B. Joshi, B. Ren, and X. Wang, "Electrochemical surface-enhanced Raman spectroscopy," Nature Reviews Methods Primers **3**, 1–21 (2023).

[31]R. J. Gale, *Spectroelectrochemistry: theory and practice* (Springer Science & Business Media, 2012).

[32]A. Wieckowski, C. Korzeniewski, and B. Braunschweig, *Vibrational Spectroscopy at Electrified Interfaces* (John Wiley & Sons, 2013).

[33]L. B. Dreier, C. Bernhard, G. Gonella, E. H. G. Backus, and M. Bonn, "Surface Potential of a Planar Charged Lipid–Water Interface. What Do Vibrating Plate Methods, Second Harmonic and Sum Frequency Measure?" The Journal of Physical Chemistry Letters **9**, 5685–5691 (2018).

[34]X. X. Han, R. S. Rodriguez, C. L. Haynes, Y. Ozaki, and B. Zhao, "Surface-enhanced Raman spectroscopy," Nature Reviews Methods Primers **1**, 1–17 (2022).

[35]B. Rehl, E. Ma, S. Parshotam, E. L. DeWalt-Kerian, T. Liu, F. M. Geiger, and J. M. Gibbs, "Water Structure in the Electrical Double Layer and the Contributions to the Total Interfacial Potential at Different Surface Charge Densities," Journal of the American Chemical Society **144**, 16338–16349 (2022).

[36]M. M. Uddin, M. S. Azam, and D. K. Hore, "Variable-Angle Surface Spectroscopy Reveals the Water Structure in the Stern Layer at Charged Aqueous Interfaces," Journal of the American Chemical Society **146**, 11756–11763 (2024).

[37]J. R. Macdonald and C. A. Barlow Jr, "Theory of double-layer differential capacitance in electrolytes," The Journal of Chemical Physics **36**, 3062–3080 (1962).

[38]D. C. Grahame, "The electrical double layer and the theory of electrocapillarity." Chemical reviews **41**, 441–501 (1947).

[39]M. Gouy, "Sur la constitution de la charge électrique à la surface d'un électrolyte," J. Phys. Theor. Appl. **9**, 457–468 (1910).

[40]E. Moreau, T. Paillat, and G. Touchard, "Space charge density in dielectric and conductive liquids flowing through a glass pipe," Journal of Electrostatics **51**, 448–454 (2001).

[41]T. Paillat, E. Moreau, and G. Touchard, "Space charge density at the wall in the case of heptane flowing through an insulating pipe," Journal of Electrostatics **53**, 171–182 (2001).

[42]A. Ndour, S. Holé, P. Leblanc, and T. Paillat, "Direct observation of electric charges at solid/liquid interfaces with the pressure-wave-propagation method," Journal of Electrostatics **109**, 103527 (2021).

[43]V. Berry, P. Leblanc, S. Holé, and T. Paillat, "Space charge measurement at solid/liquid interface by pwp method," Journal of Electrostatics **128**, 103894 (2024).

[44]K.-i. Ataka, T. Yotsuyanagi, and M. Osawa, "Potential-dependent reorientation of water molecules at an electrode/electrolyte interface studied by surface-enhanced infrared

absorption spectroscopy," The Journal of Physical Chemistry **100**, 10664–10672 (1996).

[45]M. Fleischmann, P. Hendra, I. Hill, and M. Pemble, "Enhanced raman spectra from species formed by the coadsorption of halide ions and water molecules on silver electrodes," Journal of Electroanalytical Chemistry and Interfacial Electrochemistry **117**, 243–255 (1981).

[46]C.-Y. Li, J.-B. Le, Y.-H. Wang, S. Chen, Z.-L. Yang, J.-F. Li, J. Cheng, and Z.-Q. Tian, "In situ probing electrified interfacial water structures at atomically flat surfaces," Nature materials **18**, 697–701 (2019).

[47]M. Bonn, Y. Nagata, and E. H. Backus, "Molecular structure and dynamics of water at the water–air interface studied with surface-specific vibrational spectroscopy," Angewandte Chemie International Edition **54**, 5560–5576 (2015).

[48]P. Kolb, D. Rath, R. Wille, and W. Hansen, "An esca study on the electrochemical double layer of emersed electrodes," Berichte der Bunsengesellschaft für physikalische Chemie **87**, 1108–1113 (1983).

[49]D. M. Kolb, "Electrochemical surface science," Angewandte Chemie International Edition **40**, 1162–1181 (2001).

[50]M. A. Brown, Z. Abbas, A. Kleibert, R. G. Green, A. Goel, S. May, and T. M. Squires, "Determination of surface potential and electrical double-layer structure at the aqueous electrolyte-nanoparticle interface," Physical Review X **6**, 011007 (2016).

[51]M. A. Brown, A. Goel, and Z. Abbas, "Effect of electrolyte concentration on the stern layer thickness at a charged interface," Angewandte Chemie **128**, 3854–3858 (2016).

[52]M. Favaro, B. Jeong, P. N. Ross, J. Yano, Z. Hussain, Z. Liu, and E. J. Crumlin, "Unravelling the electrochemical double layer by direct probing of the solid/liquid interface," Nature communications **7**, 12695 (2016).

[53]M. J. Bedzyk, G. M. Bommarito, M. Caffrey, and T. L. Penner, "Diffuse-double layer at a membrane-aqueous interface measured with x-ray standing waves," Science **248**, 52–56 (1990).

[54]C. B. Duke, "Surface science: the first thirty years," Surface Science **299**, vii–viii (1994).

[55]G. A. Somorjai and Y. Li, *Introduction to surface chemistry and catalysis* (John Wiley & Sons, 2010).

[56]W.-T. Liu and Y. R. Shen, "In situ sum-frequency vibrational spectroscopy of electrochemical interfaces with surface plasmon resonance," Proceedings of the National Academy of

Sciences **111**, 1293–1297 (2014).

[57]N. G. Rey and D. D. Dlott, "Studies of electrochemical interfaces by broadband sum frequency generation," Journal of Electroanalytical Chemistry **800**, 114–125 (2017).

[58]G. Lu, A. Lagutchev, D. D. Dlott, and A. Wieckowski, "Quantitative vibrational sum-frequency generation spectroscopy of thin layer electrochemistry: Co on a pt electrode," Surface Science **585**, 3–16 (2005).

[59]J. N. Israelachvili and R. M. Pashley, "Molecular layering of water at surfaces and origin of repulsive hydration forces," Nature **306**, 249–250 (1983).

[60]K. Suzuki, N. Oyabu, K. Kobayashi, K. Matsushige, and H. Yamada, "Atomic-resolution imaging of graphite–water interface by frequency modulation atomic force microscopy," Applied Physics Express **4**, 125102 (2011).

[61]A. M. Smith, A. A. Lee, and S. Perkin, "The electrostatic screening length in concentrated electrolytes increases with concentration," The journal of physical chemistry letters **7**, 2157–2163 (2016).

[62]M. A. Gebbie, A. M. Smith, H. A. Dobbs, G. G. Warr, X. Banquy, M. Valtiner, M. W. Rutland, J. N. Israelachvili, S. Perkin, R. Atkin, *et al.*, "Long range electrostatic forces in ionic liquids," Chemical communications **53**, 1214–1224 (2017).

[63]H.-J. Butt, M. Jaschke, and W. Ducker, "Measuring surface forces in aqueous electrolyte solution with the atomic force microscope," Bioelectrochemistry and Bioenergetics **38**, 191–201 (1995).

[64]S. May, "Differential capacitance of the electric double layer: Mean-field modeling approaches," Current Opinion in Electrochemistry Fundamental and Theoretical Electrochemistry 108 Physical and Nanoelectrochemistry, **13**, 125–131 (2019).

[65]K. Ojha, K. Doblhoff-Dier, and M. T. M. Koper, "Double-layer structure of the Pt(111)–aqueous electrolyte interface," Proceedings of the National Academy of Sciences **119**, e2116016119 (2022).

[66]K. Doblhoff-Dier and M. T. M. Koper, "Electric double layer of Pt(111): Known unknowns and unknown knowns," Current Opinion in Electrochemistry **39**, 101258 (2023).

[67]A. J. Bard, L. R. Faulkner, and H. S. White, *Electrochemical methods: fundamentals and applications* (John Wiley & Sons, 2022).

[68]H. A. Stern and S. E. Feller, "Calculation of the dielectric permittivity profile for a nonuniform system: Application to a lipid bilayer simulation," The Journal of Chemical

Physics **118**, 3401–3412 (2003).

[69]R. Netz and H. Orland, "Beyond Poisson-Boltzmann: Fluctuation effects and correlation functions," The European Physical Journal E **1**, 203–214 (2000).

[70]B. Zhuang and Z.-G. Wang, "Statistical field theory for polar fluids," The Journal of Chemical Physics **149**, 124108 (2018).

[71]H. Berthoumieux, G. Monet, and R. Blossey, "Dipolar Poisson models in a dual view," The Journal of Chemical Physics **155**, 024112 (2021).

[72]R. Blossey and R. Podgornik, "A comprehensive continuum theory of structured liquids," Journal of Physics A: Mathematical and Theoretical **56**, 025002 (2023).

[73]R. Blossey and R. Podgornik, "Field theory of structured liquid dielectrics," Physical Review Research **4**, 023033 (2022).

[74]G. Jeanmairet, B. Rotenberg, D. Borgis, and M. Salanne, "Study of a water-graphene capacitor with molecular density functional theory," The Journal of chemical physics **151** (2019).

[75]D. Borgis, D. Laage, L. Belloni, and G. Jeanmairet, "Dielectric response of confined water films from a classical density functional theory perspective," Chemical Science **14**, 11141–11150 (2023).

[76]M. Su and Y. Wang, "A brief review of continuous models for ionic solutions: The Poisson–Boltzmann and related theories," Communications in Theoretical Physics **72**, 067601 (2020).

[77]M. Z. Bazant, B. D. Storey, and A. A. Kornyshev, "Double layer in ionic liquids: Overscreening versus crowding," Physical review letters **106**, 046102 (2011).

[78]M. McEldrew, Z. A. H. Goodwin, A. A. Kornyshev, and M. Z. Bazant, "Theory of the Double Layer in Water-in-Salt Electrolytes," The Journal of Physical Chemistry Letters **9**, 5840–5846 (2018).

[79]J. P. de Souza and M. Z. Bazant, "Continuum Theory of Electrostatic Correlations at Charged Surfaces," The Journal of Physical Chemistry C **124**, 11414–11421 (2020).

[80]J. de Souza, A. A. Kornyshev, and M. Z. Bazant, "Polar liquids at charged interfaces: A dipolar shell theory," The Journal of Chemical Physics **156**, 244705 (2022).

[81]O. Björneholm, M. H. Hansen, A. Hodgson, L.-M. Liu, D. T. Limmer, A. Michaelides, P. Pedevilla, J. Rossmeisl, H. Shen, G. Tocci, E. Tyrode, M.-M. Walz, J. Werner, and H. Bluhm, "Water at Interfaces," Chemical Reviews **116**, 7698–7726 (2016).

[82]R. Sundararaman, D. Vigil-Fowler, and K. Schwarz, "Improving the Accuracy of Atomistic Simulations of the Electrochemical Interface," Chemical Reviews **122**, 10651–10674 (2022).

[83]E. Santos and W. Schmickler, "Models of Electron Transfer at Different Electrode Materials," Chemical Reviews **122**, 10581–10598 (2022).

[84]G. Jeanmairet, B. Rotenberg, and M. Salanne, "Microscopic Simulations of Electrochemical Double-Layer Capacitors," Chemical Reviews **122**, 10860–10898 (2022).

[85]A. Groß and S. Sakong, "Ab Initio Simulations of Water/Metal Interfaces," Chemical Reviews **122**, 10746–10776 (2022).

[86]X.-H. Yang, Y.-B. Zhuang, J.-X. Zhu, J.-B. Le, and J. Cheng, "Recent progress on multiscale modeling of electrochemistry," WIREs Computational Molecular Science **12**, e1559 (2022).

[87]L. Zeng, J. Peng, J. Zhang, X. Tan, X. Ji, S. Li, and G. Feng, "Molecular dynamics simulations of electrochemical interfaces," The Journal of Chemical Physics **159**, 091001 (2023).

[88]S.-J. Shin, D. H. Kim, G. Bae, S. Ringe, H. Choi, H.-K. Lim, C. H. Choi, and H. Kim, "On the importance of the electric double layer structure in aqueous electrocatalysis," Nature Communications **13**, 174 (2022).

[89]K. Takahashi, H. Nakano, and H. Sato, "Accelerated constant-voltage quantum mechanical/molecular mechanical method for molecular systems at electrochemical interfaces," The Journal of Chemical Physics **157**, 234107 (2022).

[90]A. Farahvash, M. Agrawal, A. P. Willard, and A. A. Peterson, "The influence of solvent on surface adsorption and desorption," (2024), arXiv:2405.18263 [physics].

[91]J. Behler and M. Parrinello, "Generalized Neural-Network Representation of High-Dimensional Potential-Energy Surfaces," Physical Review Letters **98**, 146401 (2007).

[92]O. T. Unke, S. Chmiela, H. E. Sauceda, M. Gastegger, I. Poltavsky, K. T. Schütt, A. Tkatchenko, and K.-R. Müller, "Machine Learning Force Fields," Chemical Reviews **121**, 10142–10186 (2021).

[93]J. Vandermause, S. B. Torrisi, S. Batzner, Y. Xie, L. Sun, A. M. Kolpak, and B. Kozinsky, "On-the-fly active learning of interpretable Bayesian force fields for atomistic rare events," npj Computational Materials **6**, 1–11 (2020).

[94]D. M. Anstine and O. Isayev, "Machine Learning Interatomic Potentials and Long-Range Physics," The Journal of Physical Chemistry A **127**, 2417–2431 (2023).

[95]A. Musaelian, S. Batzner, A. Johansson, L. Sun, C. J. Owen, M. Kornbluth, and B. Kozinsky, "Learning local equivariant representations for large-scale atomistic dynamics," Nature Communications **14**, 579 (2023).

[96]S. Izvekov, A. Mazzolo, K. VanOpdorp, and G. A. Voth, "Ab initio molecular dynamics simulation of the Cu(110)–water interface," The Journal of Chemical Physics **114**, 3248–3257 (2001).

[97]S. Izvekov and G. A. Voth, "Ab initio molecular dynamics simulation of the Ag(111)-water interface," The Journal of Chemical Physics **115**, 7196–7206 (2001).

[98]O. M. Magnussen and A. Groß, "Toward an Atomic-Scale Understanding of Electrochemical Interface Structure and Dynamics," Journal of the American Chemical Society **141**, 4777–4790 (2019).

[99]V. M. Sánchez, M. Sued, and D. A. Scherlis, "First-principles molecular dynamics simulations at solid-liquid interfaces with a continuum solvent," The Journal of chemical physics **131** (2009).

[100]X.-H. Yang, Y.-B. Zhuang, J.-X. Zhu, J.-B. Le, and J. Cheng, "Recent progress on multiscale modeling of electrochemistry," WIREs Computational Molecular Science **12**, e1559 (2022).

[101]J.-B. Le, X.-H. Yang, Y.-B. Zhuang, M. Jia, and J. Cheng, "Recent Progress toward Ab Initio Modeling of Electrocatalysis," The Journal of Physical Chemistry Letters **12**, 8924–8931 (2021).

[102]K. Schwarz and R. Sundararaman, "The electrochemical interface in first-principles calculations," Surface Science Reports **75**, 100492 (2020).

[103]M. M. Melander, "Grand canonical ensemble approach to electrochemical thermodynamics, kinetics, and model Hamiltonians," Current Opinion in Electrochemistry **29**, 100749 (2021).

[104]P. Lindgren, G. Kastlunger, and A. A. Peterson, "Electrochemistry from the atomic scale, in the electronically grand-canonical ensemble," The Journal of Chemical Physics **157**, 180902 (2022).

[105]C. Zhang, T. Sayer, J. Hutter, and M. Sprik, "Modelling electrochemical systems with finite field molecular dynamics," Journal of Physics: Energy **2**, 032005 (2020).

[106]J. I. Siepmann and M. Sprik, "Influence of surface topology and electrostatic potential on water/electrode systems," The Journal of chemical physics **102**, 511–524 (1995).

[107]S. K. Reed, O. J. Lanning, and P. A. Madden, "Electrochemical interface between an ionic liquid and a model metallic electrode," The Journal of chemical physics **126** (2007).

[108]S. K. Reed, P. A. Madden, and A. Papadopoulos, "Electrochemical charge transfer at a metallic electrode: A simulation study," The Journal of Chemical Physics **128**, 124701 (2008).

[109]A. P. Willard, S. K. Reed, P. A. Madden, and D. Chandler, "Water at an electrochemical interface—a simulation study," Faraday discussions **141**, 423–441 (2009).

[110]A. Marin-Laflèche, M. Haefele, L. Scalfi, A. Coretti, T. Dufils, G. Jeanmairet, S. Reed, A. Serva, R. Berthin, C. Bacon, S. Bonella, B. Rotenberg, P. A. Madden, and M. Salanne, "MetalWalls: A Classical Molecular Dynamics Software Dedicated to the Simulation of Electrochemical Systems," (2020), 10/ghbskf.

[111]G. Jeanmairet, B. Rotenberg, D. Borgis, and M. Salanne, "Study of a water-graphene capacitor with molecular density functional theory," The Journal of Chemical Physics **151**, 124111 (2019).

[112]L. Scalfi, D. T. Limmer, A. Coretti, S. Bonella, P. A. Madden, M. Salanne, and B. Rotenberg, "Charge fluctuations from molecular simulations in the constant-potential ensemble," Physical Chemistry Chemical Physics **22**, 10480–10489 (2020).

[113]Y. Zhang, H. B. de Aguiar, J. T. Hynes, and D. Laage, "Water Structure, Dynamics, and Sum-Frequency Generation Spectra at Electrified Graphene Interfaces," The Journal of Physical Chemistry Letters **11**, 624–631 (2020).

[114]Y. Zhang, G. Stirnemann, J. T. Hynes, and D. Laage, "Water dynamics at electrified graphene interfaces: A jump model perspective," Physical Chemistry Chemical Physics **22**, 10581–10591 (2020).

[115]L. Scalfi, T. Dufils, K. G. Reeves, B. Rotenberg, and M. Salanne, "A semiclassical Thomas–Fermi model to tune the metallicity of electrodes in molecular simulations," The Journal of Chemical Physics **153**, 174704 (2020).

[116]T. R. Gingrich and M. Wilson, "On the ewald summation of gaussian charges for the simulation of metallic surfaces," Chemical Physics Letters **500**, 178–183 (2010).

[117]A. P. Thompson, H. M. Aktulga, R. Berger, D. S. Bolintineanu, W. M. Brown, P. S. Crozier, P. J. In't Veld, A. Kohlmeyer, S. G. Moore, T. D. Nguyen, *et al.*, "Lammps-a

flexible simulation tool for particle-based materials modeling at the atomic, meso, and continuum scales," Computer Physics Communications **271**, 108171 (2022).

[118]H. J. Berendsen, J.-R. Grigera, and T. P. Straatsma, "The missing term in effective pair potentials," Journal of Physical Chemistry **91**, 6269–6271 (1987).

[119]A. H. Mao and R. V. Pappu, "Crystal lattice properties fully determine short-range interaction parameters for alkali and halide ions," The Journal of chemical physics **137** (2012).

[120]A. P. Willard, S. K. Reed, P. A. Madden, and D. Chandler, "Water at an electrochemical interface—a simulation study," Faraday Discussions **141**, 423–441 (2008).

[121]A. Limaye, D. Suvlu, and A. P. Willard, "Water molecules mute the dependence of the double-layer potential profile on ionic strength," Faraday Discussions **249**, 267–288 (2024).

[122]M. Dinpajooh and D. V. Matyushov, "Dielectric constant of water in the interface," The Journal of Chemical Physics **145** (2016).

[123]B. Tran, Y. Zhou, M. J. Janik, and S. T. Milner, "Negative dielectric constant of water at a metal interface," Physical review letters **131**, 248001 (2023).

[124]S. Ghosh, A. V. Soudackov, and S. Hammes-Schiffer, "Electrochemical electron transfer and proton-coupled electron transfer: Effects of double layer and ionic environment on solvent reorganization energies," Journal of chemical theory and computation **12**, 2917–2925 (2016).